PHYSICAL REVIEW B VOLUME 2, NUMBER 8 15 OCTOBER 1970

Fermi Surface of Osmium

G. N. Kamm
Naval Research Laboratory, Washington, D. C. 20390

and

J. R. Anderson
University of Maryland, College Park, Maryland 20742
(Received 1 June 1970)

The Fermi surface for osmium is found to bear a close relationship to that for ruthenium, with corresponding areas comparable or smaller. The de Haas–van Alphen frequencies observed fall into two distinct ranges differing by a factor of about 50, the higher centered at 1.5×10^8 G. The energy bands calculated for rhenium with a Fermi energy appropriate for osmium suggest a Fermi surface consisting of three large sheets – a pair of nested electron-type surfaces and an open hexagonal network of hole-type arms. Our measurements clearly detect each of these surfaces. We observe additionally a single set of small ellipsoids. If these ellipsoids are hole surfaces located on faces of the Brillouin zone near U, only minor modifications of the bands calculated for rhenium are required to bring the Fermi surface into agreement with the experimental results.

I. INTRODUCTION

As a result of extensive investigation over the last decade, the Fermi surfaces of many metals have been determined. In the present work we report our de Haas–van Alphen (dHvA) results on osmium, thus adding to the list of metals for which the Fermi surface has been determined in some detail.

Osmium has the hexagonal close-packed structure with room-temperature lattice constants $a_0 = 2.7354$ Å, and $c_0 = 4.3193$ Å.[1] Thus $c/a = 1.579$ which is slightly smaller than the ideal ratio of 1.633. Since osmium is in the same column of the Periodic Table as ruthenium, we expect results very similar to those found by Coleridge for ruthenium.[2,3] In addition, osmium is next to rhenium in the same row of the Periodic Table and since both metals have the hexagonal-close-packed (hcp) structure, we anticipate that the energy bands of osmium will be similar to those calculated by Mattheiss[4] for rhenium. As a result, the Fermi surface of osmium would be obtained from the rhenium results after taking account of the shift in the Fermi energy due to the additional valence electron. In the following, we will explicitly show these analogies with both ruthenium and rhenium.

In Sec. II the results from the dHvA theory, as applicable to our experiment, are summarized. In Sec. III the experimental technique is described, while the experimental results are given in Sec. IV. In Sec. V the applicable energy-band structure and a Fermi-surface model, based upon the rhenium band calculation, are presented. In Sec. VIII the results are summarized and compared with the results in ruthenium.

II. dHvA EFFECT SUMMARY

From a study of dHvA oscillation frequencies F, one is able to determine extremal cross-sectional area sections of the Fermi surface A using the relation[5]

$$F = \hbar cA/2\pi e\,. \tag{1}$$

Here $\hbar$, c, and e are Planck's constant over 2π, the velocity of light, and the electronic charge, respectively.

Lifshitz and Kosevich[6] have shown that the fundamental oscillatory component of the magnetization due to a particular extremal cross section is given by

$$M_{\rm osc} \propto (kT/\sqrt{H}\,)\sin(2\pi F/H \pm \pi/4 - 2\pi\gamma) \times [\cos(\pi/2)g\mu\,(\sinh\lambda\mu T/H)^{-1} e^{-\lambda\mu\chi/H}]\,. \tag{2}$$

Here $\lambda = 2\pi^2 mck/e\hbar$, k is Boltzmann's constant, and μ is the cyclotron mass ratio, $\mu = (\hbar^2/2\pi m)(\partial A_0/\partial E)$. In this expression, we have included the collision broadening term $e^{-\lambda\mu\chi/H}$,[7,8] where $\chi = \hbar/2\pi k\tau$ is an effective temperature referred to as the Dingle temperature and τ is the lifetime of a state at the Fermi energy. The term $\cos\pi g\mu/2$ is a spin-splitting term where g is the splitting factor and may differ from the free-electron value of 2.0023 because of spin-orbit effects. For our experiments in osmium, $(\sinh\lambda\mu T/H)^{-1}$ can be approximated as $2e^{-\lambda\mu T/H}$ to an accuracy of better than 1%. Thus we see that μ can be determined from a measurement of $\ln(V/T)$ as a function of T, where V is the measured signal amplitude with field modulation which is proportional to $M_{\rm osc}$. In addition, once

μ is known, χ can be determined from measurements of V as a function of H. Thus from a study of only dHvA oscillations, we are able to determine the Fermi surface, and measure the cyclotron masses and the scattering times for selected orbits on the Fermi surface.

III. EXPERIMENTAL PROCEDURE

A. Sample Preparation

The crystals used in this study were grown at the Naval Research Laboratory by B. C. La Roy and R. Williams from pressed and sintered rods of high-purity powdered osmium in an ultrahigh-vacuum electron-beam zone-refining furnace. After a number of passes to outgas the material, three melting zone passes were made at a pressure of 10^{-8} Torr. The crystals grown were about 5 in. long and roughly $\frac{1}{4}$ in. in diameter but quite irregular. Only small portions were substantially free of low-angle grain boundaries, and from these sections specimen crystals were cut by spark erosion machining. The resistivity ratio $R_{300\,^\circ\mathrm{K}}/R_{4.2\,^\circ\mathrm{K}}$ of the portions of the crystals used was about 500. The samples were cylinders about 2 mm in diameter and 5 mm long. After spark cutting, the samples were electroetched in a dilute HCl solution (1 part HCl to 3 parts H_2O). The osmium crystal was made the anode while the cathode was stainless steel. With a low-current density, blaze planes were developed on $\{10\bar{1}0\}$ crystal faces which aided in the initial orientation and also in the evaluation of the crystalline perfection of the rods grown.

B. Field Modulation Technique

dHvA oscillations were studied by means of the field modulation technique first described by Shoenberg and Stiles.[9] Thus the sample was the core of a transformer, whose primary, the modulation coil, typically consisted of 50 000 turns of No. 48 AWG wire. The secondary, or pickup coil, was a compensated coil of 2200 turns, plus 1100 balancing turns, all of No. 48 AWG wire.

Both the specimen and pickup coil were mounted in a drum which could be rotated in the plane of the magnetic field over $\pm 140^\circ$ by means of a spiral gear.[10]

The crystal was aligned with the axis of the superconducting solenoid to an accuracy of better than 1° by x-ray techniques. A check on the alignment was usually possible from the rotation diagrams at fixed magnetic field. From such studies, we have concluded that the plane of rotation could be specified to within $\frac{1}{2}^\circ$–1°.

The modulation frequency was normally 100 Hz and the dHvA signal was picked up at either this fundamental frequency or the second harmonic and detected with phase-sensitive techniques. The final result was displayed on an x-y recorder. The amplitude of the ac modulation field was automatically maintained accurately proportional to the square of the sweeping field,[11] that is, a constant proportion of a dHvA period, by means of a system of ganged potentiometers and a pair of operational amplifiers. This was required for measurements of the Dingle temperature and was frequently useful in maintaining maximum enhancement of a particular dHvA frequency.

C. Magnetic Fields

The dHvA effect was studied in a conventional iron magnet having a maximum field capability of 25 kOe and in two superconducting solenoids, one a Westinghouse Nb-Zr 55-kOe magnet and the other a 100-kOe Nb-Sn magnet (in these experiments almost never used above 75 kOe). Since most of our results were obtained with the 100-kOe magnet, this system is described here in greater detail.

It is well known that superconducting solenoids, constructed of niobium-tin alloy, exhibit pronounced hysteresis effects, not only in the relation of magnetic current to central field, but also in the field uniformity through the central region. Accordingly, the measurement of the magnetic field must be made not by the solenoid current but by some independent method. For both the 100-kOe superconducting solenoid and the iron magnet, the magnetic field was determined by sensing the flux change as the field was swept with a fixed sensing coil whose axis was parallel to the field direction. The output of this coil was integrated by a low-leakage polystyrene-type capacitor together with a low-drift operational amplifier.[12] In order to use this technique satisfactorily, it was necessary to establish the zero of field either at the beginning of the experiment with the solenoid normal or with the magnet de-Gaussed with ac current. No significant change in the zero reading was detected over the course of an experiment of several hours duration except as noted below.

For the superconducting magnet, the flux sensing coil was also the 50 000-turn modulation coil. In order to ensure that this dc field measuring signal was isolated from the modulation generation system, the modulation was introduced to the common coil through capacitative coupling. Unfortunately, with this common-coil technique the modulation amplitude was limited to a maximum of about 40 Oe by magnetoresistance effects in the copper wire which produced an extra effective dc voltage proportional to the square of the modulation field. The result of this extra voltage is the equivalent of a drift in field reading and a progressive error in dc field. This source of drift could have been

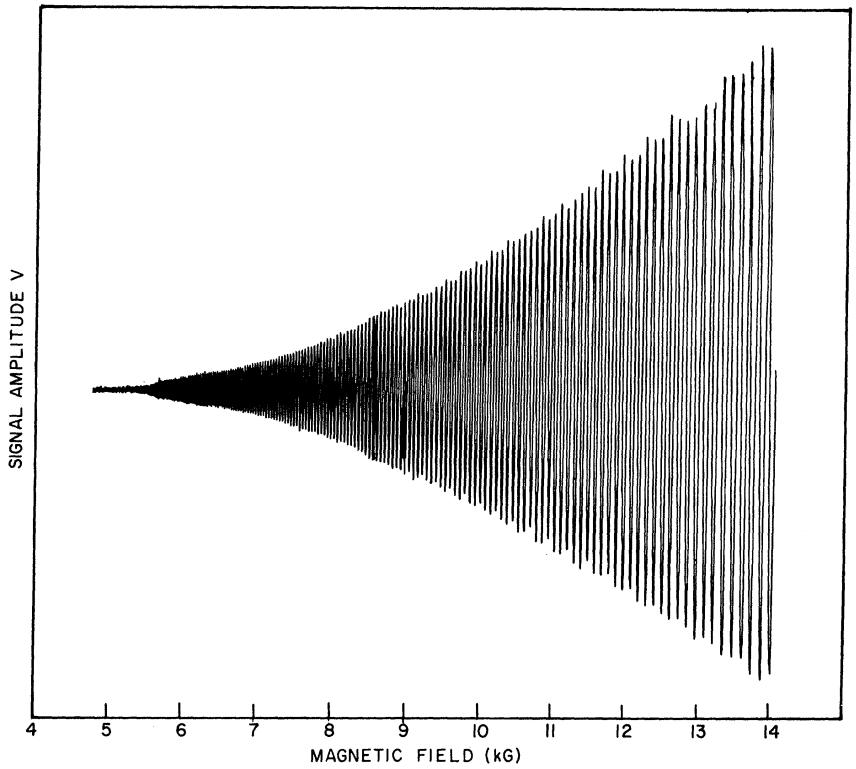

FIG. 1. Typical low-frequency dHvA oscillations in osmium. For the $\langle 10\bar{1}0\rangle$ direction signal strength, V is plotted as a function of magnetic field. With the modulation field kept proportional to H^2, the amplitude variation with field is used for the determination of the Dingle temperature. Principal component corresponds in Fig. 2 to point b, while the smaller amplitude component with a beat of about 3 cycles corresponds to point d.

eliminated and a higher modulation field achieved by the use of separate coils for field modulation and flux sensing. The fluxmeter calibration was established using nuclear magnetic resonance (NMR) with a small specimen containing H^1, F^{19}, and Al^{27} (powdered metal) nuclei located as closely as possible (within $\frac{1}{2}$ in.) below the sample rotator. In a calibration, the NMR specimen would be centered and the field set to exact resonance, then the dHvA specimen and flux coils centered and the fluxmeter reading noted. (The magnet power supply has sufficient stability, better than 1 part in 10^5 per hour, to remain on an NMR resonance for a long period.) With this technique the magnetic field could be measured to about 0.5%.

The field was not swept uniformly as is usually done. Instead, it was set to a prominent maximum of the dHvA oscillation pattern, the peak was marked, and its reading from a digital voltmeter noted. Then the field was swept at an arbitrary rate over a large number of cycles and stopped at the next marking point, the peak noted, and the field recorded, and the process repeated as desired. This method of recording avoids the systematic errors which could arise from the response time of the x-y recorder and the delay time of the digital voltmeter.

IV. RESULTS

The dHvA oscillations in osmium are clearly divided into two groups, the lower-frequency group having frequencies of the order of 3×10^6 G or lower and the higher with values of about 1.5×10^8 G. The former are the easiest to discuss and will be described first.

A. Low Frequencies

An example of the low-frequency oscillations for $\vec{H}$ along $[10\bar{1}0]$ is shown in Fig. 1. These frequencies, labeled α, are plotted as a function of angle in the three principal symmetry planes in Fig. 2. It can be easily shown that these frequency branches could result from a single set of closed surfaces which have been designated class C by Watts.[13] Each closed surface would have the symmetry characteristic of one of the points M, L, S, T, R, U, Σ, S', or T' (Fig. 3). From comparisons with band calculations, referred to in Sec. V, we suggest that these surfaces are centered between the points L and M on the center line of a side face of the hexagonal zone.

The dependence of frequency on orientation suggests that the small pieces are ellipsoidal in form. The experimental frequencies were fitted to an ellipsoidal model as indicated by the solid curves of Fig. 2. Obviously the fit, and therefore the ellipsoidal approximation, is very good. In Table I we summarize for all of the oscillations the dHvA frequencies, the effective masses, and the Dingle temperatures at symmetry points. From the fre-

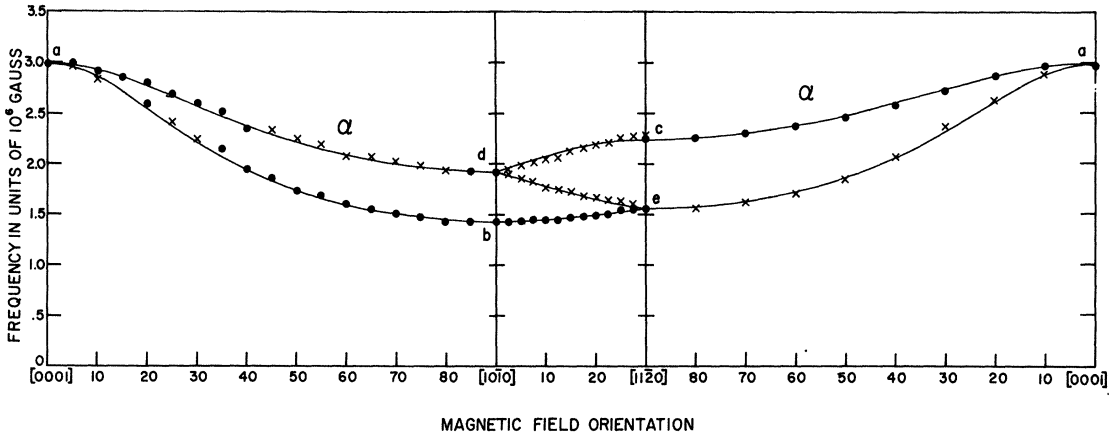

FIG. 2. Angular variation of the low-frequency dHvA oscillations α. Experimental points denoted by circles are the principal components. Those denoted by crosses have been determined from the pattern of beats and are therefore somewhat less reliable. Solid curves represent the fitted ellipsoid.

quencies at points a, b, and c the resulting cross-sectional areas are determined by Eq. (1), and from them in turn, the principal axes which are listed in Table II. Cyclotron masses for the ellipsoids are plotted as a function of the Fermi-surface extremal areas in Fig. 4. The approximately linear relation suggests that not only is this part of the Fermi surface ellipsoidal, but also that a quadratic dependence of energy upon wave vector is a good approximation.

Dingle temperatures were determined from the dependence of magnetization upon field at constant temperature. A sample of such data for the ellipsoids is shown in Fig. 1. The measured Dingle temperatures were about 0.8 °K for one specimen and 0.5 °K for another. These values are comparable to Dingle temperatures found with the same specimens for the larger sheets (see Table I and Sec. IV B). Beyond indicating the quality of the specimens, this suggests that, for these field directions, the surfaces in question do not exhibit magnetic breakdown, at least up to 15 kG. The relaxation time, determined from a Dingle temperature of 0.8 °K as indicated in Sec. II, is 2.1×10^{-12} sec. Another estimate of the relaxation time is possible by assuming that the two $6S$ electrons in the atomic configuration of osmium are free and by applying the relation $\tau = m/Ne^2\rho$ where m is the electronic mass, N is the density of free electrons, and ρ is the measured resistivity (by the eddy-current decay method).[14] This value of relaxation time is $1.4_3\times10^{-12}$ sec. In view of the rough nature of the assumptions the agreement is satisfactory.

B. High Frequencies

Next simplest to discuss after the lowest-frequency oscillation, attributed to small ellipsoids, are the highest frequencies observed, β and γ. Typical of these oscillations are those shown in Fig. 5, for H along ⟨0001⟩. These form two independent

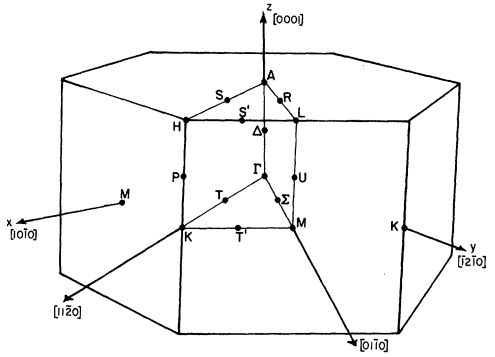

FIG. 3. Brillouin zone for the hexagonal structure with symmetry points and lines labeled according to the standard notation.

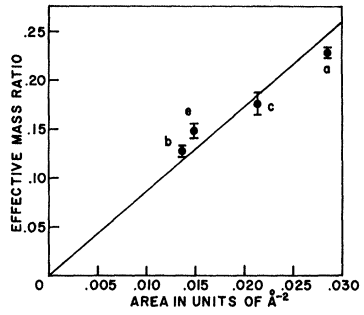

FIG. 4. Plot of effective masses from Table I as a function of extremal areas as determined from the low-frequency dHvA oscillations. Proportionality suggests that energy is a quadratic function of wave vector.

TABLE I. dHvA frequencies, effective masses, and Dingle temperatures for symmetry directions.

Fermi-surface sheet	Direction	Oscillation nomenclature group	dHvA frequency (10^6 G)	Cyclotron mass ratio (μ)	Dingle temp. (°K)
h_7 hole ellipsoids	$\langle 0001\rangle$	α_a[a]	$2.9_9 \pm 0.02$	$0.22_8 \pm 0.005$	0.49 ± 0.05
	$\langle 10\bar{1}0\rangle$	α_b[a]	$1.4_3 \pm 0.01$	$0.12_8 \pm 0.006$	0.76 ± 0.06
	$\langle 11\bar{2}0\rangle$	α_c[a]	$2.2_4 \pm 0.02$	$0.17_6 \pm 0.012$	
	$\langle 11\bar{2}0\rangle$	α_e[a]	$1.5_5 \pm 0.01$	$0.14_9 \pm 0.007$	0.84 ± 0.06
e_{10} smaller of nested electron surfaces	$\langle 0001\rangle$	β (max.)	153 ±1.5	$1.2_5 \pm 0.10$	0.3 est.
	$\langle 0001\rangle$	β (waist)	148 ±1.5		
	$\langle 10\bar{1}0\rangle$	β	$124_8 \pm 1.5$	$1.2_6 \pm 0.10$	
	$\langle 11\bar{2}0\rangle$	β	$133_8 \pm 1.5$		
e_9 larger of electron surfaces	$\langle 0001\rangle$	γ	$205_3 \pm 2.0$		
	$\langle 10\bar{1}0\rangle$	γ	160 ±8.0		
	$\langle 11\bar{2}0\rangle$	γ	168 ±13		
h_8 hole arms	$\langle 10\bar{1}0\rangle$	δ	110 ±1.5	1.49 ±0.04	
	$\langle 11\bar{2}0\rangle$	δ	109 ±1.5	1.10 ±0.03	$0.8_6 \pm 0.15$
	$\langle 11\bar{2}0\rangle$	ϵ	68 ±1.0	1.1 est.	

[a]Letters refer to identification in Fig. 2.

branches, each of which apparently extend over all angles as shown in Fig. 6. The oscillations could not be followed over the entire angular range because at some orientations the amplitudes become weak compared to competing oscillations. However, we have assumed that the branches could be continued as indicated by the dashed lines in Fig. 6. Thus we find that these oscillations represent closed surfaces and since they are of similar form, we believe one is nested within the other. We also note that the patterns are very similar for magnetic field rotations in $(10\bar{1}0)$ and $(11\bar{2}0)$ planes, implying that the surfaces have approximately circular symmetry about the hexagonal axis. Watts[13] has characterized such oscillations as "class A" based upon their symmetry pattern, and consequently the resulting surfaces must be centered about Γ, A, K, H, or Δ. Based upon the band calculations to be

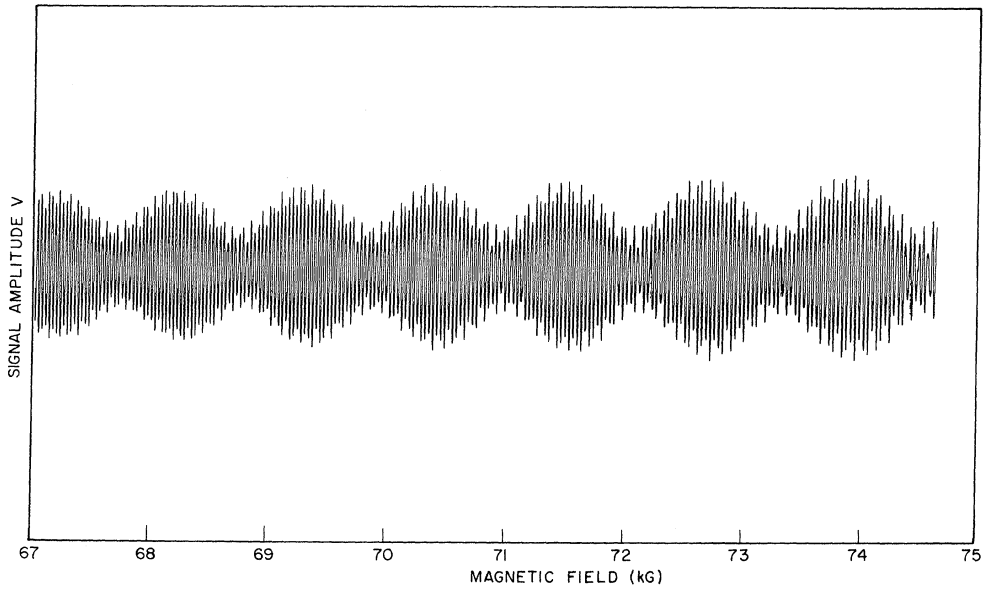

FIG. 5. Typical high-frequency oscillations in osmium. Signal strength is plotted as a function of field in the $\langle 0001\rangle$ direction. Two frequencies producing the long period beat of about 32 cycles are associated with the waisted electron sheet e_{10}, while the more rapid but weaker beat is associated with sheet e_9 together with e_{10}.

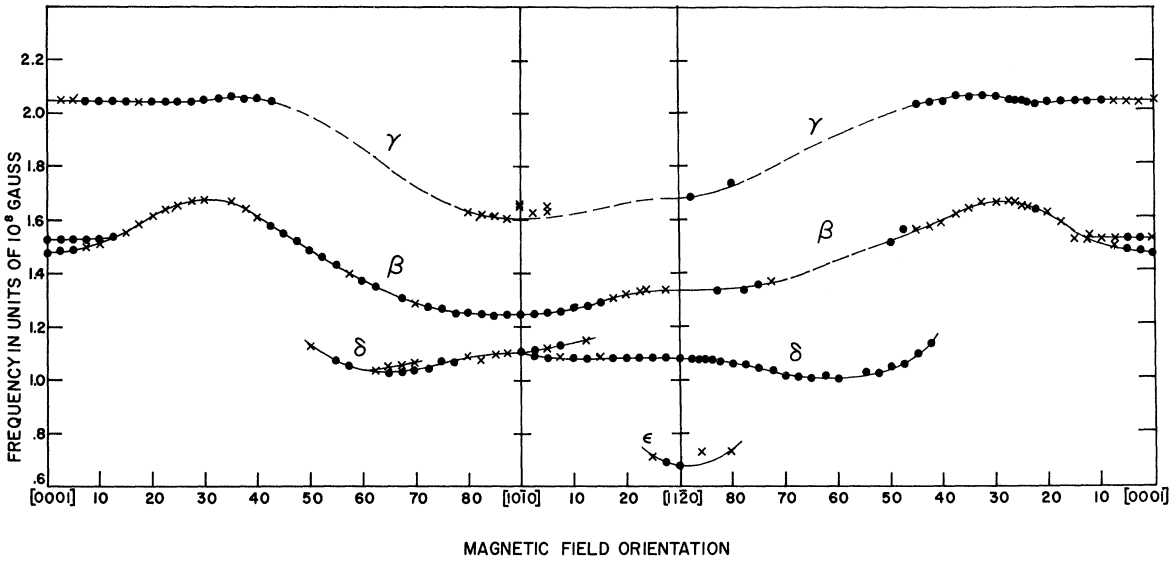

FIG. 6. Angular variation of the higher-frequency dHvA oscillations. Experimental points denoted by circles are the principal component, while those denoted by crosses have been determined from beating oscillations and in general are somewhat less reliable. Dashed lines are the presumed extensions of the branches at angles where the amplitudes of oscillations were either too low to be followed or were obscured by other oscillations of larger amplitude.

described in Sec. V, and from the large sizes of both surfaces, we assume that both are centered at Γ.

For the smaller of the two surfaces, a distinct beating pattern is observed for field angles within 13° of ⟨0001⟩; this suggests that the surface is waisted as shown in Fig. 7.

The intermediate-frequency oscillations δ, Fig. 6, form branches lying in and near the basal plane, but not extending to the ⟨0001⟩ directions. We note the degeneracy at ⟨10$\bar{1}$0⟩, and the separation of the two branches as the magnetic field is rotated from ⟨10$\bar{1}$0⟩ toward ⟨11$\bar{2}$0⟩. This behavior suggests that the δ oscillations do not result from closed surfaces but from a multiply connected surface of ⟨11$\bar{2}$0⟩ arms. In addition, there is a lower branch of oscillations ϵ observed near ⟨11$\bar{2}$0⟩. We suggest that the ⟨11$\bar{2}$0⟩ arms have a minimum cross section in addition to the central maximum section, and that the ϵ branch results from this part of the Fermi surface.

Effective mass ratios for the higher-frequency oscillations are included in Table I. It can be seen from Fig. 4 that for the case of the small ellipsoids, a larger extremal cross section corresponded to a larger mass ratio. A similiar behavior is observed for the δ oscillations which arise from h_8, the sheet of hole arms. For the field along ⟨11$\bar{2}$0⟩ parallel to an arm axis the mass ratio for the maximal area is 1.10 while with the field rotated 30° in the basal plane to ⟨10$\bar{1}$0⟩ the ratio increases to 1.5. But for the smaller of the electron sheets, e_{10}, the mass ratio for the field along ⟨10$\bar{1}$0⟩ is 1.2_6, while for the field along ⟨0001⟩ where the area is maximum the ratio is essentially unchanged at 1.2_5.

V. FERMI-SURFACE MODEL

Although there have been no band-structure calculations for osmium (at. no. 76), Mattheiss[4] has calculated the energy bands for its neighbor, rhenium (at. no. 75). Rhenium is also hexagonal and close packed with a c/a ratio of 1.613, which is nearly the same as that of osmium. Computations were made both with and without relativistic corrections, but the closest correlation with the rhenium dHvA measurements resulted from the inclusion of relativistic corrections including spin-orbit coupling. Therefore, we assume relativistic corrections are required for osmium as well. In Fig. 8 we show the rhenium energy bands of Mattheiss but with the Fermi energy determined for one additional electron corresponding to osmium. The calculated density-of-states–versus–energy curve[4] was used

TABLE II. Dimensions of the ellipsoidal hole surfaces.

Measured direction	Radial semiaxis (Å^{-1})	Brillouin-zone dimension (Å^{-1})		Ratio
⟨0001⟩ (L toward M)	$0.057_1 \pm 0.0004$	(L-M)	0.7288	0.00783
⟨10$\bar{1}$0⟩ (L toward A)	$0.119_0 \pm 0.0008$	(L-A)	1.329	0.0895
⟨11$\bar{2}$0⟩ (L toward H)	$0.076_3 \pm 0.0005$	(L-H)	0.7672	0.0995

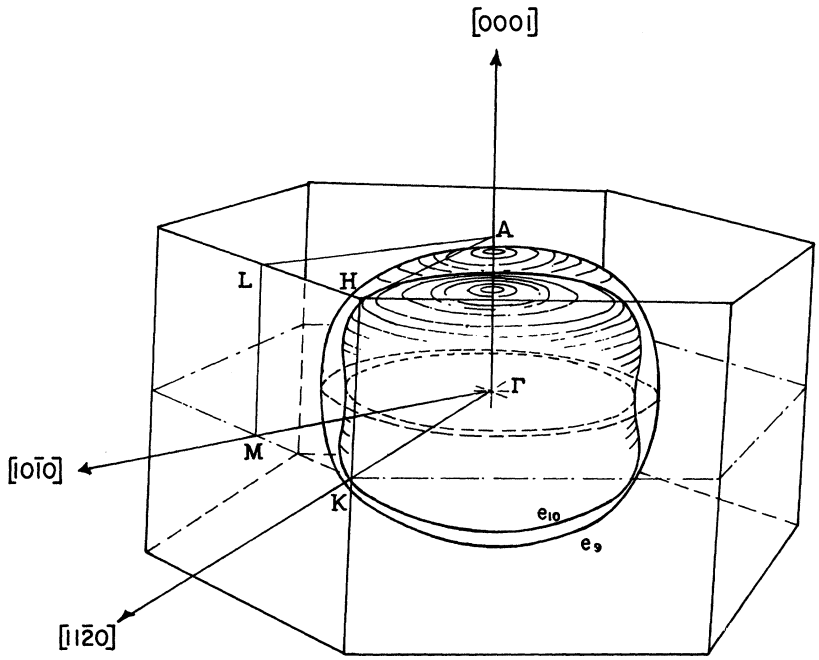

FIG. 7. Perspective view of the nested pair of electron-type Fermi-surface sheets e_9 and e_{10}. Their cross section in the basal plane is shown in Fig. 10.

to position the Fermi level. An expanded section of the bands along the lines M-L-H is shown in Fig. 9, which will be of significance to a later argument.

The large features of the Fermi surface predicted from the band calculation are essentially the same with and without the inclusion of spin-orbit coupling. They consist of two large electron sheets in the ninth and tenth zones, e_9 and e_{10}, centered at Γ,

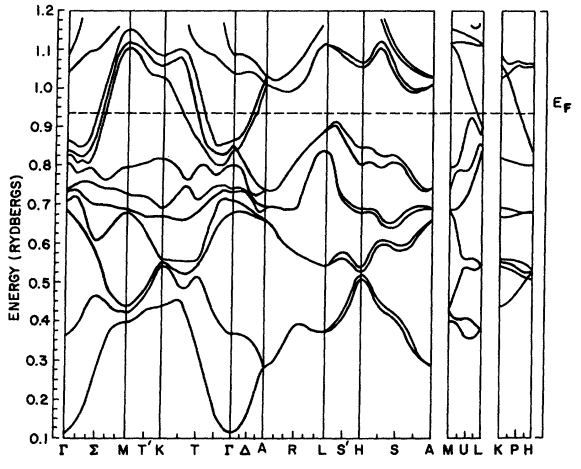

FIG. 8. Band structure calculated for rhenium by Mattheiss including relativistic and spin-orbit corrections. Fermi level appropriate to osmium was determined from the integrated density of states. (See Ref. 4).

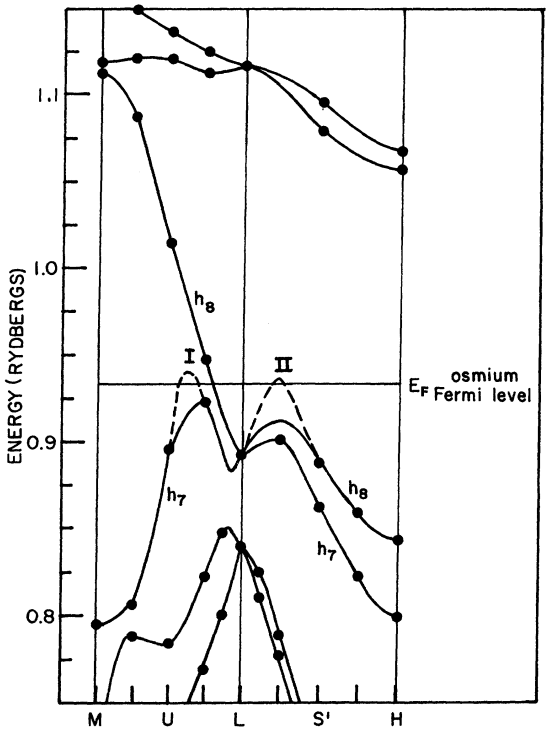

FIG. 9. Expanded section of the energy bands along the lines M-L and L-H. Points and solid curves are from Ref. 4. Dashed curves indicate modifications which would be sufficient for the appearance at point I of sheet h_7 of hole ellipsoids of the size experimentally observed, and at point II of a small contact region with the Brillouin zone which could give rise to open orbits in the ⟨0001⟩ direction.

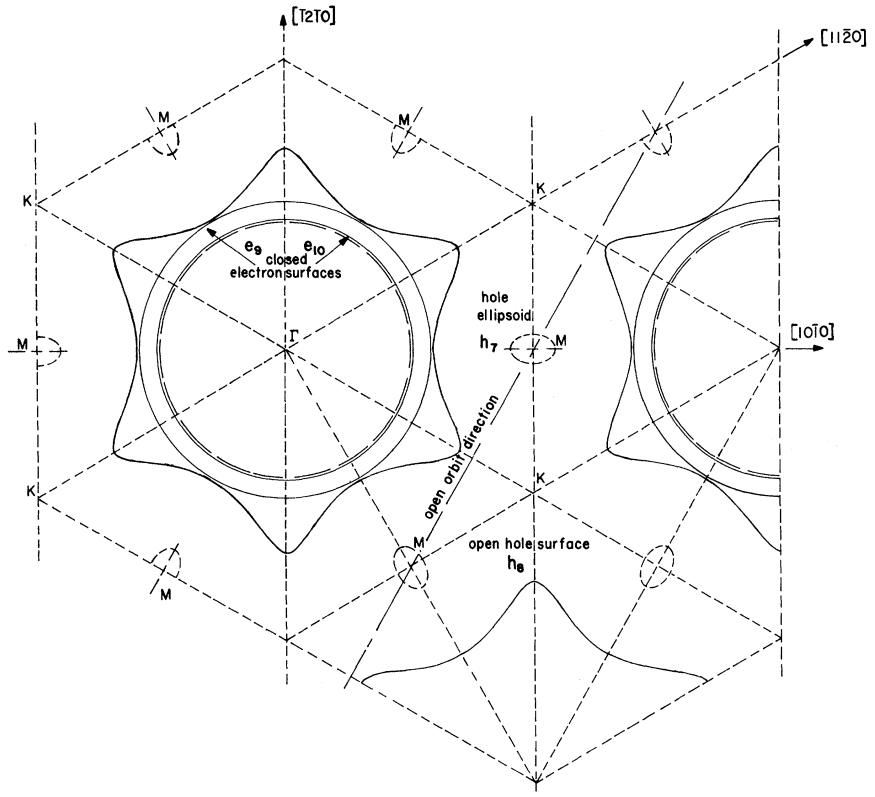

FIG. 10. Cross section through Γ perpendicular to ⟨0001⟩ of a model of the Fermi surface of osmium suggested by the band structure and consistent with the the experimental dHvA results. Shown dashed are projections on this basal plane of the small h_7 ellipsoidal surfaces and of typical open orbits in a ⟨10$\bar{1}$0⟩ direction.

and a large hole surface in the eighth zone, h_8. Without the spin-orbit coupling the two electron sheets touch, but this contact is removed with the inclusion of the spin-orbit correction. As we noted in Sec. IV, oscillations γ and β are related to large closed pieces of Fermi surface. These must correspond to the two large nested electron sheets e_9 and e_{10}. In addition, the δ oscillations appear to result from ⟨11$\bar{2}$0⟩ branches in the basal plane corresponding to the large multiply connected eighth-zone hole surface h_8 which encloses the symmetry

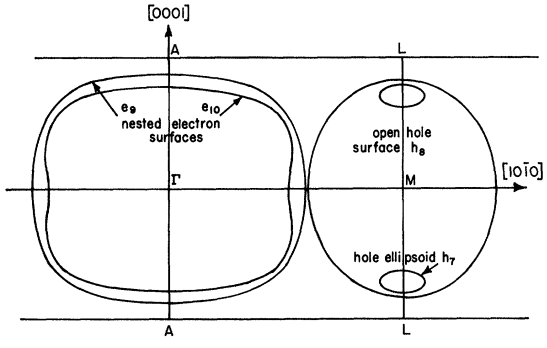

FIG. 11. Cross section of the Fermi surface in a plane perpendicular to ⟨11$\bar{2}$0⟩ passing through points Γ, A, L, and M.

points K and M but not Γ or A. There are several experimental features by which these oscillations can be attributed to h_8. The oscillations cease to exist at field angles approaching ⟨0001⟩ (Fig. 6). In addition, the oscillations were observed closer to [0001] in the plane of rotation from [11$\bar{2}$0] to [0001] than in the plane of rotation from [10$\bar{1}$0] to [0001]. This fact plus the degeneracy and branching observed for $\vec{H}\parallel\langle 10\bar{1}0\rangle$ strongly suggest a hexagonal structure of ⟨11$\bar{2}$0⟩ arms. In addition, the ϵ oscillations observed for $\vec{H}$ near ⟨11$\bar{2}$0⟩ can be explained as resulting from a minimum arm cross section centered between M and K, as discussed in Sec. IV.

The three large pieces of Fermi surface are easily distinguished in the band structure. For example, one notes three intersections with the Fermi surface between the points Γ-M and Γ-K. However, there are only two intersections between Γ-A and none between A-L. In Fig. 10 are drawn intersections with the basal plane of these three sections of the Fermi surface constructed to be consistent with our experiment dHvA results. (Oscillations from the striking 6-pointed star-shaped region of h_8 have not been observed, perhaps because the effective mass is nearly twice that for e_9. Under the conditions of the experiment, the amplitude would be lower by a factor of about 20.) The same surfaces are represented intersecting the ΓMLA plane in Fig. 11,

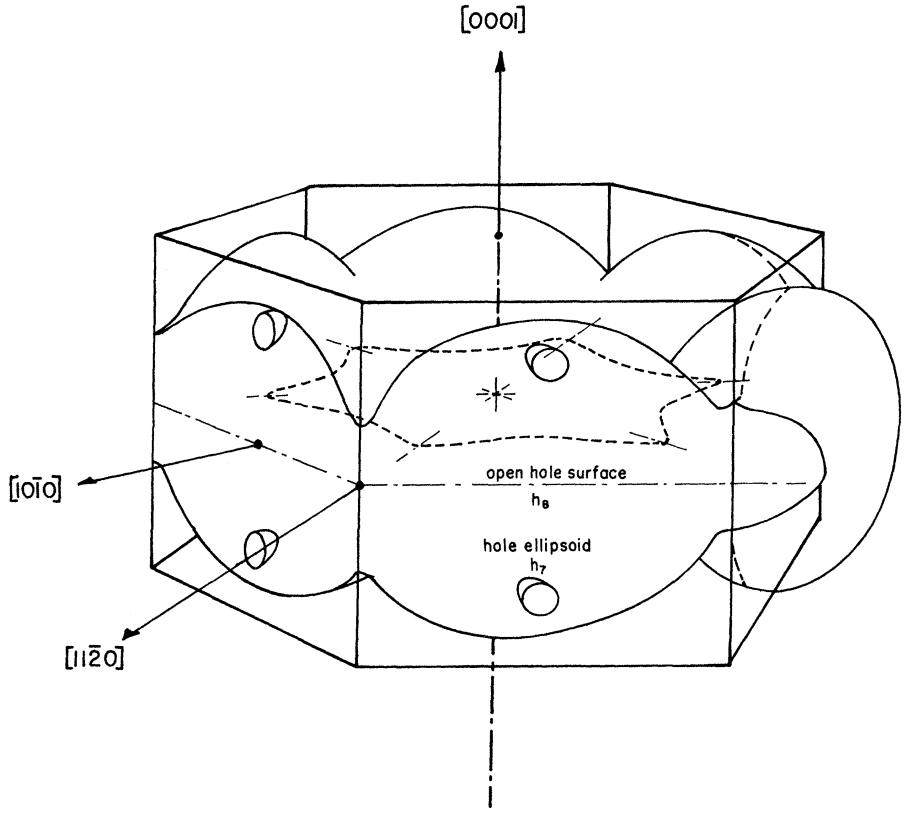

FIG. 12. Perspective view of the hole-type Fermi-surface sheets. Surface h_8 forms an interconnected network of arms lying along $\langle 11\bar{2}0\rangle$ directions. Ellipsoidal surfaces h_7 are shown located on a line between L and M.

which shows the two large electron surfaces and the hole surface $[\bar{1}2\bar{1}0]$ arm cross section. For clarity, an over-all view of this hole surface is shown in Fig. 12. We see that this surface does not extend all the way to L. Because all levels are twofold degenerate at L, this lack of hole-surface contact at L will be important to our discussion of the lower-frequency dHvA oscillations below.

The α oscillations result from nearly ellipsoidal pieces of Fermi surface, and no such small segments are apparent in the Mattheiss model. However, only slight modifications would produce ellipsoids centered on the line L-M corresponding to holes in the seventh zone h_7. In fact, such pieces would even be consistent with the actual points calculated by Mattheiss as illustrated at point I in Fig. 9. The spin-orbit coupling eliminates contact between h_7 and h_8 so that h_7 lies entirely within h_8, as shown in Figs. 8 and 9. This fact is consistent with our Dingle-temperature measurements which show no abrupt changes in dHvA amplitudes for the α oscillations.

VI. CORRELATION WITH MAGNETORESISTANCE

Osmium, as a consequence of its even number of valence electrons and hexagonal structure, is expected to be a compensated metal. As a result, it is expected that the magnetoresistance will vary quadratically for a general magnetic field direction. This expected behavior has been observed in the magnetoresistance measurements of Alekseevskii *et al.*[15] Furthermore, for $\vec{H}$ perpendicular to $\langle 10\bar{1}0\rangle$ saturation of the magnetoresistance was observed indicating open-orbit paths along this direction. Such open orbits are possible, resulting from the hole-surface network h_8. In a projection on the basal plane, such orbits would appear as passing through successive points M as shown in Fig. 10. In addition, the magnetoresistance data show a slight dip for $\vec{H}\perp\langle 0001\rangle$ (much smaller than that for $\vec{H}\perp\langle 10\bar{1}0\rangle$ suggesting the existence of open orbits along $\langle 0001\rangle$. This is not possible according to the model we have shown since such open orbits would require the sheet h_8 to make contact with the AHL plane of the Brillouin zone. However, slight changes could produce this contact near but not exactly at L. The contact cannot be at L if we attribute the strong oscillations δ for $\vec{H}\parallel\langle 11\bar{2}0\rangle$ to the h_8 arm sections centered at M. The calculated band structure also indicates that if the level of h_8 were shifted to give contact with the AHL plane, the contact would not occur at L but perhaps along the line L-H at point II, as suggested in Fig. 9. If such contact were to occur, we might expect a

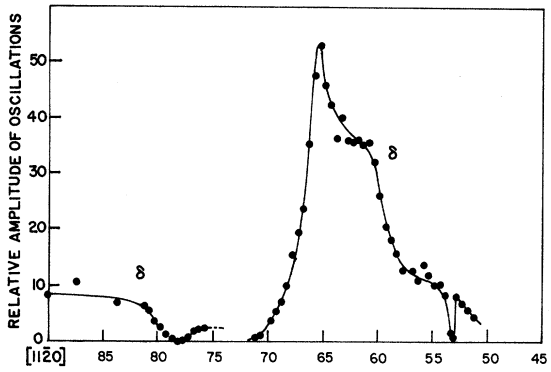

FIG. 13. Variation of signal amplitude for the δ oscillations for field rotation in the (10$\bar{1}$0) plane.

gap in our δ oscillation data for H rotated away from the basal plane about 10°. Although we have not definitely found such gaps in the data, the dHvA amplitudes behave peculiarly in that region. In Fig. 13 we have plotted the amplitude as a function of field orientation for rotation in a $\{10\bar{1}0\}$ plane, and we note a null at 12° from $\langle 11\bar{2}0\rangle$. Thus our dHvA data do suggest that open orbits exist along $\langle 0001\rangle$ directions.

In addition to the null in the δ oscillations at 12° from [11$\bar{2}$0], Fig. 13 shows a sharp null at an angle 53° from [0001]. The amplitudes are also complex for a field rotation in the basal plane as illustrated by Fig. 14, which shows sharp nulls in the δ oscillations at $5\frac{1}{2}$° and 16° from [11$\bar{2}$0]. These features have not been fully explained. The nulls do not arise from zeros of the Bessel function factor[11] which multiplies the magnetization when the field modulation method is used, nor do we believe they result from crystalline imperfections of the specimens. Since it seems unlikely that these δ oscillation nulls are related to a variation of the g factor for this surface, and further, since the γ oscillations have small amplitude at these orientations, the nulls may reflect points at which magnetic breakdown occurs between the surfaces h_8 and e_9. This would be most likely to occur near the basal, or ΓMK, plane.

VII. COMPARISON WITH RUTHENIUM

Coleridge[2,3] has made a fairly complete investigation of ruthenium which is quite similar to osmium. The main difference arises from the smaller spin-orbit splitting to be expected in ruthenium. In ruthenium there are large nested electron surfaces similar to e_9 and e_{10}. In addition, Coleridge found a multiply connected hole surface which he calls λ and which is like our surface h_8. His oscillations ω might well also be due to λ resulting from a minimum arm cross section; we have made this associ-

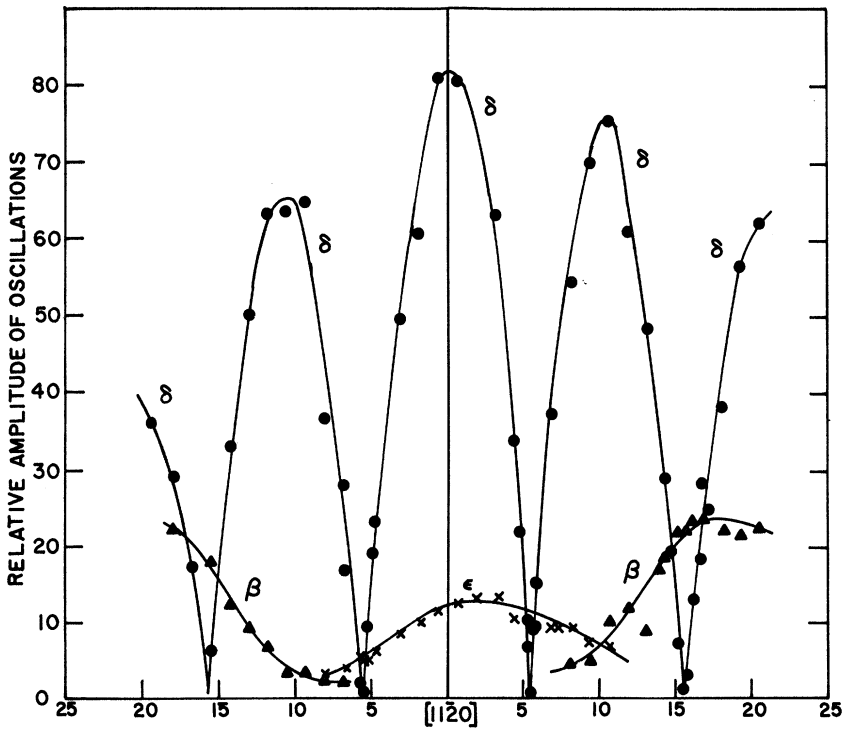

FIG. 14. Variation of signal amplitude in the (0001) plane for the δ, ϵ, and β oscillations.

ation with h_8 for the ϵ oscillations in osmium,

As might be expected, the smaller pieces of Fermi surface are somewhat different in the two metals. Coleridge[3] sees oscillations γ which he attributes to a small hole region centered at Γ. This piece is absent in osmium, probably because of the larger spin-orbit splitting. In ruthenium, there also appears to be a set of hole ellipsoids α centered at L which are not present in osmium. We believe that the ruthenium oscillations β correspond to the α oscillations in osmium which we attribute to ellipsoids centered between L and M but not enclosing the point L. We do not believe that the osmium hole surface h_8 makes contact at L and thus neither can the ellipsoids. In ruthenium, it is not clear how oscillations from central arm sections can be observed along $\langle 11\bar{2}0 \rangle$ if the surface λ encloses the point L.

VIII. CONCLUSIONS

We have determined rather completely the Fermi surface of osmium, and agreement with the rhenium band calculations of Mattheiss, with an adjusted energy level, is quite good. There are four contributions to the Fermi surface: Two nested electron surfaces centered at Γ, a multiply connected hole surface enclosing the symmetry points L-M, and small ellipsoids centered along the line L-M. These same surfaces appear to be present in ruthenium as well, but there are additional small ellipsoidal surfaces in this metal due to the smaller spin-orbit contribution. Thus, it appears as if one band calculation can be used to give good qualitative pictures of several transition metals of similar structure if the Fermi levels are determined from the plot of density of states versus energy.

ACKNOWLEDGMENTS

We wish to thank Dr. Stephen Lane for his considerable help during the initial phase of this study. We also wish to acknowledge helpful discussions with Dr. Peter Coleridge.

[1]W. B. Pearson, *A Handbook of Lattice Spacings and Structures of Metals and Alloys* (Pergamon, New York, 1958).

[2]P. T. Coleridge, Phys. Letters 22, 367 (1966).

[3]P. T. Coleridge, J. Low Temp. Phys. 1, 577 (1969).

[4]L. F. Mattheiss, Phys. Rev. 151, 450 (1966).

[5]L. Onsager, Phil. Mag. 43, 1006 (1952).

[6]I. M. Lifshitz and A. M. Kosevich, Zh. Eksperim. i Teor. Fiz. 29 730 (1955) [Soviet Phys. JETP 2, 636 (1956)].

[7]R. B. Dingle, Proc. Roy. Soc. (London) A211, 517 (1952).

[8]A. D. Brailsford, Phys. Rev. 149, 456 (1966).

[9]D. Shoenberg and P. J. Stiles, Proc. Roy. Soc. (London) A281, 62 (1964).

[10]A. C. Thorsen and T. G. Berlincourt, Rev. Sci. Instr. 34, 435 (1963).

[11]L. R. Windmiller and J. B. Ketterson, Rev. Sci. Instr. 39, 1672 (1968).

[12]Analog Devices model 232K, a chopper-stabilized type having 0.1-μV and 0.5-pA offset change per °C.

[13]B. R. Watts, Proc. Roy. Soc. (London) A282, 521 (1964).

[14]Actually, the eddy-current decay method was only used to determine a resistivity ratio. The room-temperature value was obtained from G. K. White and S. B. Woods, Phil. Trans. Roy. Soc. London, A251, 273 (1959).

[15]N. E. Alekseevskii, A. V. Dubrovin, G. E. Karstens, and N. N. Mikhailov, Zh. Eksperim. i Teor. Fiz. 54, 350 (1968) [Soviet Phys. JETP 27, 188 (1968)].